

# ON THE CALCULATION OF THE FLOW AROUND 2-D SQUARE CYLINDER WITH ROUNDED CORNERS

H. Abreu<sup>1</sup>, L. Eça<sup>1</sup> and G. Vaz<sup>2</sup>

1: Mechanical Engineering Department  
Instituto Superior Técnico  
University of Lisbon  
Av. Rovisco Pais 1, Lisbon

e-mail: hugo.abreu.91@gmail.com, luis.eca@tecnico.ulisboa.pt, web: <http://tecnico.ulisboa.pt>

2: Maritime Research Institute Netherlands  
P.O. Box 28, 6700 AA Wageningen, The Netherlands  
e-mail: G.Vaz@marin.nl, web: <http://www.marin.nl>

**Keywords:** Problem Settings, Numerical Uncertainty, Verification, Validation, RANS

**Abstract.** *This paper presents the calculation of the flow around a square cylinder with rounded-corners assuming two-dimensional and incompressible flow. The selected mathematical model is the Reynolds-Averaged (ensemble averaged) Navier-Stokes equations supplemented by the two-equation  $k - \omega$  SST eddy-viscosity turbulence model. The goal of the study is to investigate the influence of the choice of the problem settings on the prediction of several meaningful flow quantities for practical applications.*

*Two main choices are addressed in this work: the size of the computational domain and the specification of the pressure and turbulence quantities boundary conditions. The selected Reynolds number is typical of offshore applications ( $1.74 \times 10^5$ ) and grid/time refinement studies are performed for all conditions to enable the estimation of the numerical uncertainty. All calculations are performed with the (U)RANS solver ReFRESCO.*

*The results show that the level of grid/time refinement required to obtain negligible numerical uncertainties is more demanding than the typical values found in the open literature. Nonetheless, the data also show that the size of the domain and the specification of pressure and turbulence quantities (inlet) boundary conditions have a significant influence on the predicted flow quantities. Therefore, any simulation for a proper Validation procedure must follow the correct domain size and boundary conditions. Unfortunately, all this information is seldom available and so this hampers the possibility to evaluate correctly the modelling error.*

## 1 INTRODUCTION

Many practical constructions use cylinders that range from circular cross-sections to square cylinders with rounded corners. Typical Reynolds numbers of offshore applications

are in the range of  $10^5$  to  $10^6$  where the so-called "drag crisis" occurs, [1]. Flow simulations in such conditions are extremely challenging because the flow exhibits laminar, transitional and turbulent regions. Furthermore, due to the existence of vortex shedding, the flow is not statistically steady. Although many of the publications available in the open literature focus on the circular cylinder, there is a growing interest in square shapes with rounded corners [2] to [8].

Recently [9], a squared cylinder with rounded corners of 9% of the diameter has been tested in a towing tank for Reynolds numbers  $Rn$  based on the undisturbed incoming flow  $U_\infty$  and cylinder width  $D$  ranging from  $7.2 \times 10^4$  to  $3.1 \times 10^5$ . In the present paper, we address the calculation of the flow around this shape at a Reynolds number of  $1.74 \times 10^5$  assuming two-dimensional and incompressible flow. Furthermore, we have selected one of the simplest mathematical models to deal with this type of flows: the Reynolds-Averaged Navier-Stokes (RANS) equations supplemented by the eddy-viscosity Shear-Stress Transport (SST)  $k - \omega$  two-equation turbulence model [10]. Naturally, mean flow quantities are obtained by ensemble averaging because the flow is not statistically steady<sup>1</sup>.

Our goal is to investigate the influence of the problem settings on the results obtained for several meaningful flow quantities for practical applications, as for example the average drag coefficient and the maximum and root mean squared of the lift coefficient. Two main aspects are investigated in this work:

- The size of the computational domain.
- The specification of the pressure and turbulence quantities boundary conditions.

All calculations are performed with the (U)RANS solver ReFresco and grid/time refinement studies are performed for each flow condition to enable the estimation of the numerical uncertainty [11]. Naturally, the round-off and iterative components of the numerical error are reduced to negligible levels when compared to the discretization error. The outcome of the present exercise gives a clear illustration of the requirements for a reliable comparison between simulations and experiments, i.e. the information required to perform meaningful Validation exercises.

The paper is organized in the following way: the flow solver is briefly described in section 2 and the problem settings including domain size, boundary conditions, grid sets, quantities of interest and calculation details are presented in section 3; results of the grid/time refinement studies are subsequently presented and discussed in section 4, while the main conclusions are summarized in section 5.

## 2 ReFresco FLOW SOLVER

ReFresco is a viscous-flow CFD code that solves multiphase (unsteady) incompressible flows using the Navier-Stokes equations, complemented with turbulence models, cavi-

---

<sup>1</sup>This leads to the so-called URANS equations.

tation models and volume-fraction transport equations for different phases. The equations are discretized using a finite-volume approach with cell-centered collocated variables, in strong-conservation form, and a pressure-correction equation based on the SIMPLE algorithm is used to ensure mass conservation. Time integration is performed implicitly with first or second-order backward schemes. At each implicit time step, the non-linear system for velocity and pressure is linearized with Picard's method and either a segregated or coupled approach is used. A segregated approach is always adopted for the solution of all other transport equations. The implementation is face-based, which permits grids with elements consisting of an arbitrary number of faces (hexahedrals, tetrahedrals, prisms, pyramids, etc.), and if needed h-refinement (hanging nodes). State-of-the-art CFD features such as moving, sliding and deforming grids, as well automatic grid refinement are also available. For turbulence modelling, RANS/URANS, SAS and DES approaches can be used (PANS and LES are being currently studied). The code is parallelized using MPI and sub-domain decomposition, and runs on Linux workstations and HPC clusters. ReFRESCO is currently being developed and verified at MARIN (in the Netherlands) in collaboration with IST (in Portugal), USP-TPN (University of Sao Paulo, Brazil), TUDelft (Technical University of Delft, the Netherlands), UoS (University of Southampton, UK) and recently UTwente (University of Twente, the Netherlands) and Chalmers (Chalmers University, Sweden) [12].

### 3 PROBLEM SETTINGS

#### 3.1 Domain Size

The domain for the calculation of the two-dimensional flow around the rounded corner ( $r_c = 0.09D$ ) cylinder at a Reynolds number of  $1.74 \times 10^5$  is a rectangle of variable size that is illustrated in figure 1. The inlet and outlet boundaries are  $x = \text{const.}$  planes located  $L_{in}$  and  $L_{out}$  upstream and downstream of the cylinder centre, respectively. The external boundaries are  $y = \text{const.}$  planes located  $L_{ext}$  away from the cylinder centre. Three different domains were tested in the present exercise. The corresponding values of  $L_{in}$ ,  $L_{out}$  and  $L_{ext}$  are given in table 1.

#### 3.2 Boundary Conditions

Several alternatives were tested for the specification of the boundary conditions. Nonetheless, there are boundary conditions that remained fixed for all calculations:

- No-slip and impermeability conditions are applied at the cylinder surface (no wall-functions) and the normal pressure derivative is set equal to zero. The turbulence kinetic energy  $k$  is set equal to zero and  $\omega$  is specified at the near-wall cell centre [13].
- Zero stream wise derivatives are assumed for all flow variables at the outlet boundary.

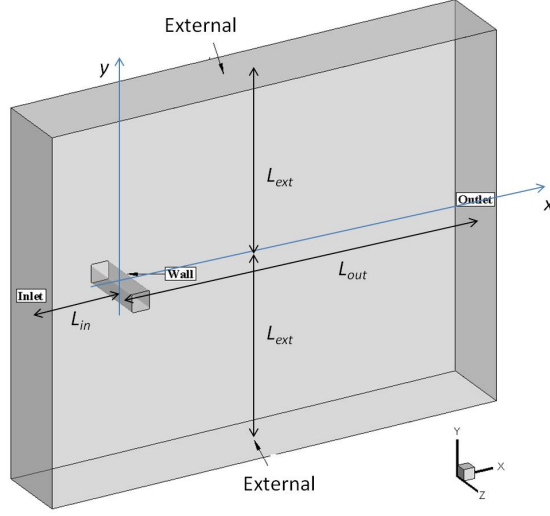


Figure 1: Domain for the calculation of the two-dimensional flow around a squared cylinder of rounded corners at  $Rn = 1.74 \times 10^5$ .

Domain	$L_{in}$	$L_{out}$	$L_{ext}$
DS	5	20	10
DM	10	40	20
DL	20	80	40

Table 1: Distances of the boundaries to the cylinder centre for the three domain sizes tested in the calculation of the two-dimensional flow around a squared cylinder with rounded corners at  $Rn = 1.74 \times 10^5$ .

- At the external boundary, zero normal derivatives have been applied to the  $x$  velocity component  $u_x$  and to the turbulence quantities  $k$  and  $\omega$ , whereas the  $y$  velocity component  $u_y$  is set equal to zero.
- At the inlet boundary,  $u_x = U_\infty$ ,  $u_y = 0$  and the pressure is extrapolated from the interior assuming zero stream wise derivative.

Two different alternatives were tested for the pressure at the external boundary:

1. Pressure equal to undisturbed flow pressure  $p_\infty$ , i.e.  $C_p = 0$ .
2. Zero normal pressure derivative and  $C_p = 0$  at the top left corner of the domain.

Three different values were tested for the turbulence quantities at the inlet boundary. The selected values of  $k$ ,  $\omega$  and the corresponding values of eddy-viscosity  $\nu_t$  and turbulence intensity  $I$  are given in table 2.

Inlet	$k/U_\infty^2$	$\omega D/U_\infty$	$\nu_t/\nu$	$I(\%)$
IL	$1.5 \times 10^{-4}$	2609.6	0.01	1
IM	$3.75 \times 10^{-3}$	6525	0.1	5
IH	$1.5 \times 10^{-2}$	2609.6	1	10

Table 2: Turbulence quantities specified at the inlet of the domain in the calculation of the two-dimensional flow around a squared cylinder with rounded corners at  $Rn = 1.74 \times 10^5$ .

It should be mentioned that the  $k$  and  $\omega$  transport equations [10] in an incoming uniform flow reduce to

$$\begin{aligned} \frac{\partial k}{\partial x} &= -\beta^* k \omega & \Rightarrow & & k &= k_{in} (1 + \beta(x - x_{in})\omega_{in})^{-\beta^*/\beta} \\ \frac{\partial \omega}{\partial x} &= -\beta \omega^2 & & & \omega &= \omega_{in} (1 + \beta(x - x_{in})\omega_{in})^{-1} \end{aligned} \quad (1)$$

where all quantities have been made dimensionless using  $D$  and  $U_\infty$  as the reference length and velocity scales, respectively. The subscript *in* designates values at the inlet boundary. The eddy-viscosity in the inflow region is given by

$$\nu_t = (\nu_t)_{in} (1 + \beta(x - x_{in})\omega_{in})^{1-\beta^*/\beta} \quad (2)$$

For the SST  $k - \omega$  model in the outer flow region [10]  $\beta^* = 0.09$  and  $\beta = 0.0828$  and so equations (1) and (2) give a rapid decay of  $k$  and  $\omega$  in the inlet region, but the value of  $\nu_t$  decays much slower than  $k$  and  $\omega$ . For example, for the inlet turbulence quantities given in table 2, 2D downstream of the inlet  $k$  is less than 1% of  $k_{in}$ , whereas  $\nu_t$  is close to 60% of the inlet value.

### 3.3 Grid Sets and Time Step

Three sets (one for each domain size) of five geometrically similar grids were generated for the simulation of the flow around a squared cylinder of rounded corners. As illustrated in figure 2, in the common part of the computational domains, DS, DM and DL, the grids are coincident and all the sets cover a grid refinement ratio  $r_i = h_i/h_1 = 2$ . The finest grid of the DS domain contains 254016 cells with 1440 cells on the cylinder surface. The maximum dimensionless distance to the wall of the near-wall cells in the coarsest grid is  $(y_2^+)_{max} < 0.3$ .

The time step of each calculation is tuned to obtain an average Courant number close to 3 that corresponds to a maximum Courant number close to 23. The time step  $\Delta t_i$  is refined with the same ratio of the grid refinement, i.e.  $r_i = \Delta t_i/\Delta t_1 = h_i/h_1$ . The dimensionless time step of the finest grids calculation is  $\Delta t U_\infty/L = 0.02083$  (roughly 335 time steps per period).

### 3.4 Quantities of Interest

The influence of the domain size and boundary conditions specification is evaluated for the following flow quantities: mean drag coefficient  $(C_D)_{avg}$ ; maximum  $(C_L)_{max}$  and

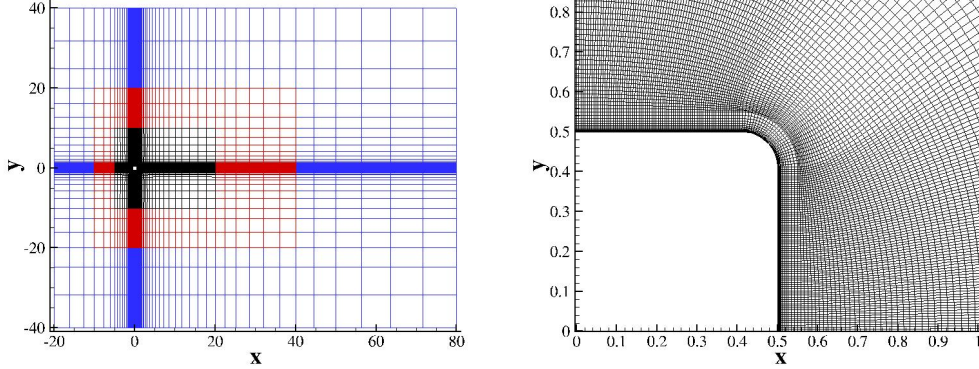


Figure 2: Illustration of the coarsest grids for the calculation of the two-dimensional flow around a squared cylinder of rounded corners at  $Rn = 1.74 \times 10^5$ .

root mean squared  $(C_L)_{rms}$  of the lift coefficient and Strouhal number  $St$ . Besides these functional quantities, we will also analyze the surface pressure  $C_p = (p - p_\infty)/(1/2\rho U_\infty^2)$  and skin friction  $C_f = \tau_w/(1/2\rho U_\infty^2)$  coefficients, where  $p_\infty$  is the undisturbed pressure and  $\tau_w$  is the shear-stress at the wall. All these flow quantities were obtained from the data of the last eight cycles performed in each calculation.

### 3.5 Calculation Details

The selected discretization schemes are all second-order accurate including the convective terms of the  $k$  and  $\omega$  transport equations. However, flux limiters are applied to all second-order upwind schemes that are used to discretize the convective terms of all equations solved. The segregated solver is used for the solution of the momentum and continuity equations at each time step.

All the calculations were performed in double precision to guarantee that the round-off error is negligible when compared to the discretization error. The iterative convergence criteria applied at each time step of the last 200 dimensionless time units requires a maximum normalized residual of all equations solved (momentum balance, mass conservation and  $k$  and  $\omega$  transport equations) below  $Res_{max} < 10^{-6}$ . The normalized residuals are equivalent to the variables change in a simple Jacobi iteration. However, to facilitate the start of the vortex shedding, all the simulations are started with 20 dimensionless time units calculated with an iterative convergence criteria of  $10^{-2}$ .

## 4 RESULTS

### 4.1 Numerical Uncertainty

#### 4.1.1 Iterative Errors

Figure 3 illustrates the typical iterative convergence results with the data obtained for the finest grid of the DM domain, the inlet conditions IM and the pressure fixed at the

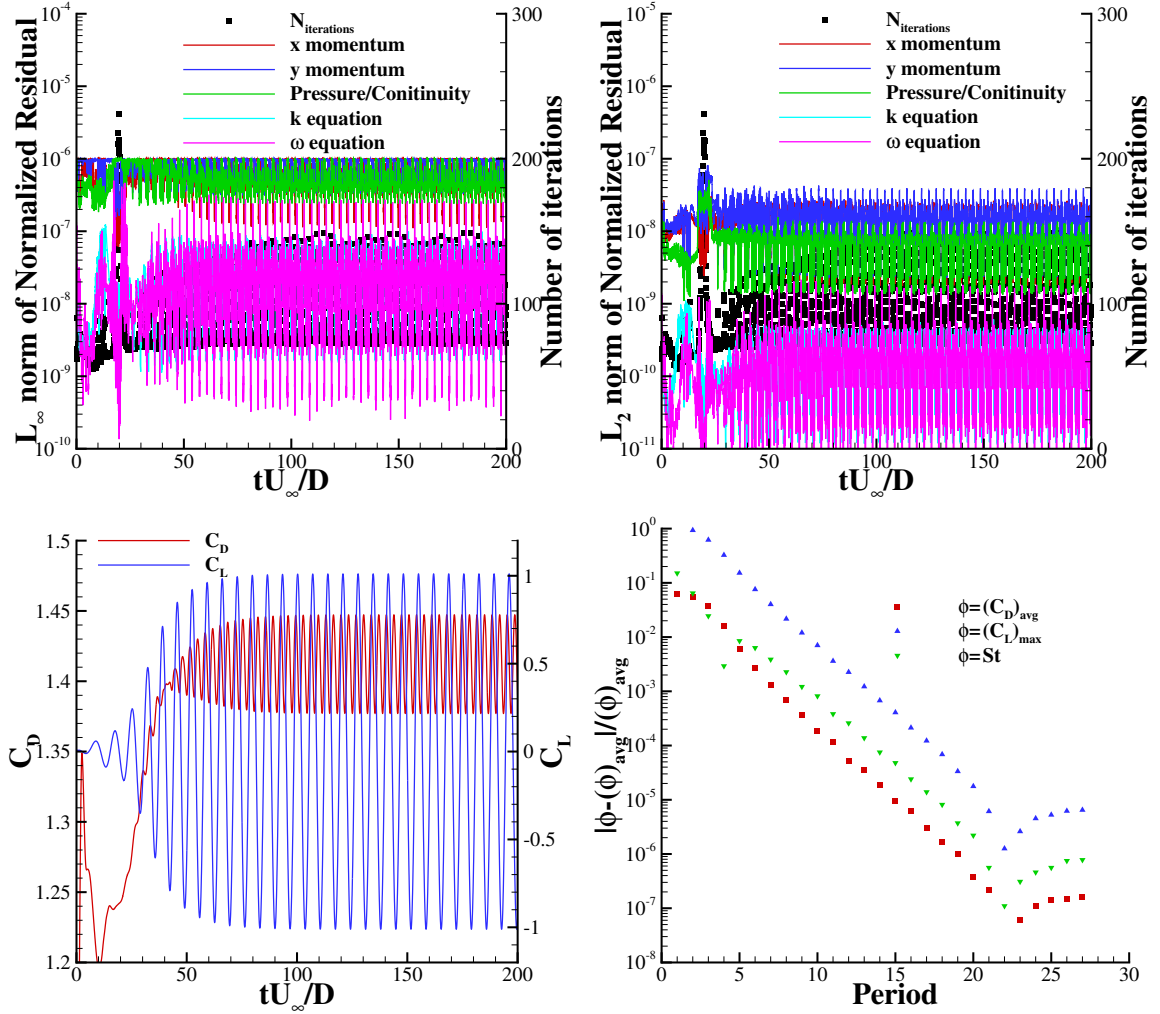


Figure 3: Illustration of the iterative convergence of the calculation of the two-dimensional flow around a squared cylinder of rounded corners at  $Rn = 1.74 \times 10^5$ .  $N_{iterations}$  is the number of iterations performed at each time step.  $\phi_{avg}$  is the value of variable  $\phi$  obtained from the average of the last 8 cycles. Finest grid of DM size with IM inlet conditions and pressure fixed at the top left corner of the domain.

top left corner of the domain. The two top plots present the  $L_2$  and  $L_\infty$  norms of the final normalized residuals of all equations solved at each time step. For the present convergence criteria ( $L_\infty$  norm smaller than  $10^{-6}$ ), the  $L_2$  norm of all normalized residuals is at least one order magnitude below the accepted tolerance. These two pictures also include the number of iterations ( $N_{iterations}$ ) performed at each time, which remains between 80 and 160 iterations when the solution becomes periodic.

The two bottom plots of figure 3 demonstrate that 200 dimensionless time units are sufficient to obtain a solution with a negligible influence of the initial condition. However, we should emphasize that the time history of  $C_D$  and  $C_L$  is not sufficient to make such

$1 \leq r_i \leq 2$ Variable	Pressure fixed at top left corner				
	DS,IL	DS, IM	DS, IH	DM, IM	DL, IM
$\Delta(C_D)_{avg}\%$	3.3	2.2	1.1	2.5	3.5
$\Delta(C_L)_{rms}\%$	3.6	8.9	16.8	3.2	1.0
$\Delta(C_L)_{max}\%$	3.5	8.9	17.0	3.2	1.0
$\Delta St\%$	2.9	2.9	2.6	2.3	2.8
$1 \leq r_i \leq 2$ Variable	Pressure fixed at external boundary				
	DL,IL	DL, IM	DL, IH	DS, IM	DM, IM
$\Delta(C_D)_{avg}\%$	4.2	3.5	2.5	2.2	3.5
$\Delta(C_L)_{rms}\%$	4.0	1.0	10.1	11.2	1.0
$\Delta(C_L)_{max}\%$	3.8	1.1	10.2	11.2	1.1
$\Delta St\%$	2.8	2.9	3.1	3.2	2.9
$1 \leq r_i \leq 1.5$ Variable	Pressure fixed at top left corner				
	DS,IL	DS, IM	DS, IH	DM, IM	DL, IM
$\Delta(C_D)_{avg}\%$	2.0	1.2	0.5	1.4	1.9
$\Delta(C_L)_{rms}\%$	1.0	3.1	6.3	0.9	0.5
$\Delta(C_L)_{max}\%$	0.7	3.2	6.0	1.0	0.5
$\Delta St\%$	1.5	1.5	1.2	1.2	1.6
$1 \leq r_i \leq 1.5$ Variable	Pressure fixed at external boundary				
	DL,IL	DL, IM	DL, IH	DS, IM	DM, IM
$\Delta(C_D)_{avg}\%$	2.5	1.9	1.2	1.2	1.9
$\Delta(C_L)_{rms}\%$	3.5	0.6	3.9	4.4	0.6
$\Delta(C_L)_{max}\%$	3.5	0.5	4.0	4.5	0.5
$\Delta St\%$	1.5	1.6	1.7	1.7	1.6

Table 3: Data range in percentage of the selected functional flow quantities of calculation of the two-dimensional flow around a squared cylinder with rounded corners at  $Rn = 1.74 \times 10^5$ .

judgement, as illustrated in the low right corner plot that compares the values obtained in each period with the average value of the last 8 cycles.

#### 4.1.2 Discretization Errors

As mentioned above, each flow condition (domain size and selected boundary conditions) is calculated with 5 systematically refined grids/time steps. Therefore, the numerical uncertainty can be estimated with the procedure proposed in [11]. However, as illustrated below, the two coarsest grids/largest time steps are too coarse to obtain reliable estimations of the numerical error with power series expansions. Unavoidably [11], the estimated uncertainties including the data of these grids will be most likely too conservative. Therefore, the figures below present the lines fitted in the least squares sense to the five data points, but we will not present the estimated error bars. Nonetheless, we



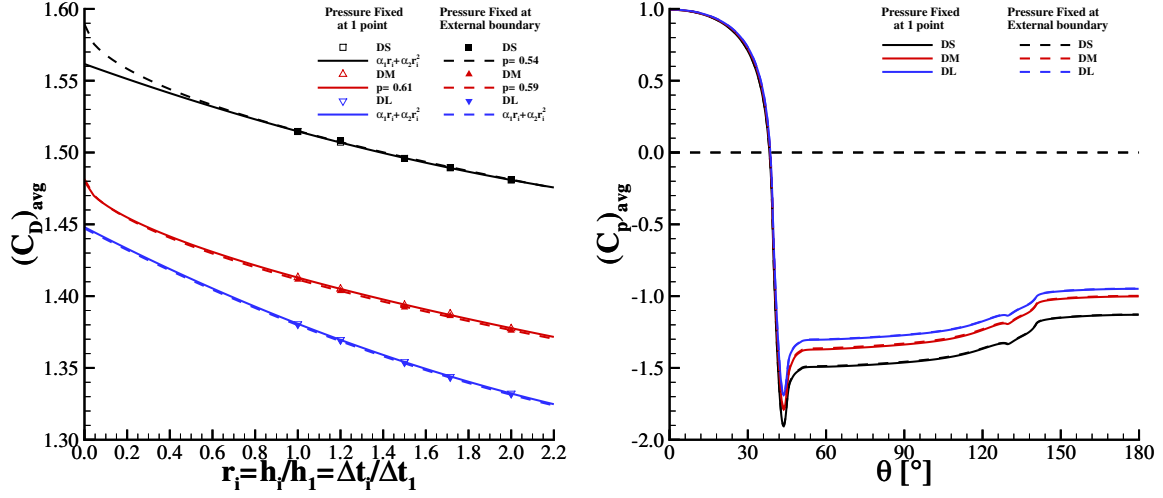


Figure 4: Average drag coefficient  $(C_D)_{avg}$  as a function of the grid/time refinement ratio (left); average surface pressure coefficient  $(C_p)_{avg}$  distribution ( $\theta = 0$  at  $x = -0.5D, y = 0$  and  $\theta = 180^\circ$  at  $x = 0.5D, y = 0$ ) for  $r_i = 1$  (right). Calculation of the two-dimensional flow around a squared cylinder of rounded corners at  $Rn = 1.74 \times 10^5$  with three different sizes of the computational domain and different pressure boundary conditions. IM inlet conditions.

present the data range of the several functional flow quantities addressed in this study in table 3. Furthermore, table 3 includes the values for  $1 \leq r_i \leq 2$  and for  $1 \leq r_i \leq 1.5$ .

The data included in table 3 show that the numerical uncertainty is not negligible for many of the flow conditions tested. Nevertheless, there is a systematic reduction of the data range when its values are calculated with  $1 \leq r_i \leq 1.5$  instead of  $1 \leq r_i \leq 2$ .

It should be mentioned that roughly 5 days of c.p.u. time are required to calculate 200 dimensionless time units in the finest grid/smallest time-step using 4 quad-cores (16 processors) of 2.6GHz. A calculation performed with the same iterative convergence criteria and  $r_i = 0.75$  took nearly 9 days. Unfortunately, for that level of grid/time refinement  $Res_{max} < 10^{-6}$  is not sufficient to obtain a negligible level of the iterative error ( $(C_L)_{avg}$  was of the order  $10^{-4}$ , whereas all the present calculations exhibit  $(C_L)_{avg} \simeq 10^{-6}$ ).

#### 4.2 Domain size and pressure boundary conditions

Figure 4 presents the average drag coefficient  $(C_D)_{avg}$  as a function of the grid/time refinement ratio  $r_i$  and the average surface pressure coefficient  $(C_p)_{avg}$  distribution for  $r_i = 1$ . Results were obtained in computational domains with three different sizes (see table 1) and two alternative pressure boundary conditions: pressure fixed at the top left corner of the domain and pressure fixed at the external boundary.

The results show a significant influence of the domain size with the difference between the  $(C_D)_{avg}$  of the smallest (DS) and largest (DL) domains reaching values close to 11%,

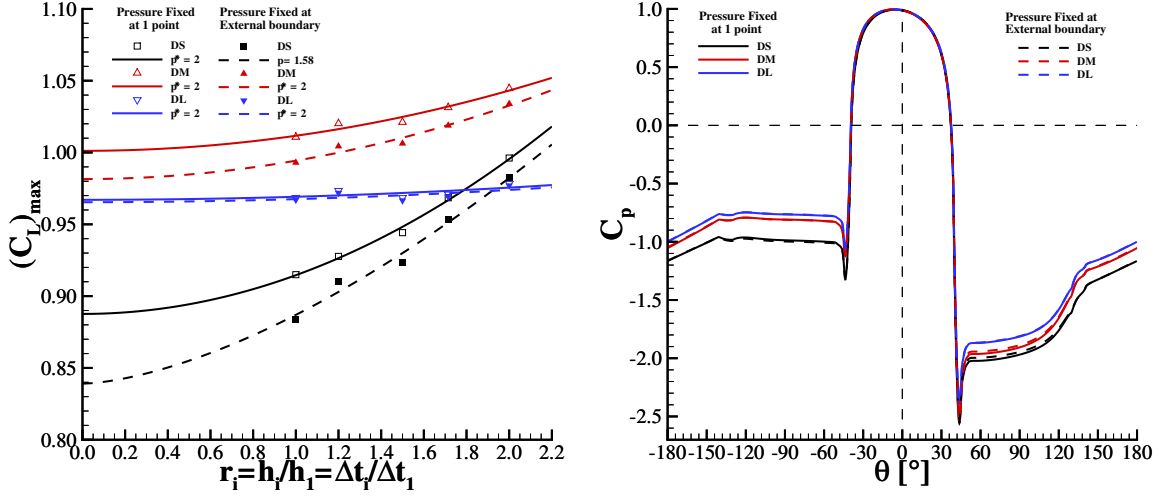


Figure 5: Maximum lift coefficient  $(C_L)_{max}$  as a function of the grid/time refinement ratio (left); surface pressure coefficient  $(C_p)_{avg}$  distribution ( $\theta = 0$  at  $x = -0.5D, y = 0$ ,  $\theta = 180^\circ$  at  $x = 0.5D, y = 0$  and  $\theta = -90^\circ$  at  $x = 0, y = -0.5D$ ) at the time corresponding to  $(C_L)_{max}$  for  $r_i = 1$  (right). Calculation of the two-dimensional flow around a squared cylinder of rounded corners at  $Rn = 1.74 \times 10^5$  with three different sizes of the computational domain and different pressure boundary conditions. IM inlet conditions.

which is significantly larger than the data range given in table 3. On the other hand, the results obtained with the two types of pressure boundary conditions are very similar for the three domain sizes. The  $(C_p)_{avg}$  distributions show that the pressure peak at the cylinder left corners and the pressure level in the flow separation region are the main origin of the discrepancies obtained in the  $(C_D)_{avg}$  predictions.

The comparison of the maximum lift coefficient  $(C_L)_{max}$  and  $C_p$  surface distributions at the time corresponding to  $(C_L)_{max}$  for the same flow conditions of the previous figure is presented in figure 5. As for  $(C_D)_{avg}$ , there is a clear influence of the domain size on the predicted  $(C_L)_{max}$ . However, in this case the change is not monotonic. The justification for such behaviour of  $(C_L)_{max}$  is given by the  $C_p$  surface distribution that shows the same trend for the pressure on the lower part of the cylinder, whereas  $C_p$  on the upper part of the cylinder exhibits a monotonic change with the domain size. On the other hand, the sharp pressure peaks at the corners of the cylinder ( $\theta = \pm 45^\circ$ ) show that it is not trivial to obtain negligible levels of discretization errors for this flow.

Figure 6 presents the skin friction coefficient  $C_f$  on the cylinder surface for the two conditions discussed above: average of a complete cycle and time corresponding to maximum lift coefficient  $(C_L)_{max}$ . The results show a small influence of the domain size and pressure boundary conditions on the friction force at the cylinder surface. The average flow exhibits separation at the corners of the cylinder without re-attachment. Naturally, at the time corresponding to  $(C_L)_{max}$  the  $C_f$  distribution is not symmetric (the stagnation point at the back of the cylinder is located at  $y \simeq -0.25D$ ), but there is no re-attachment

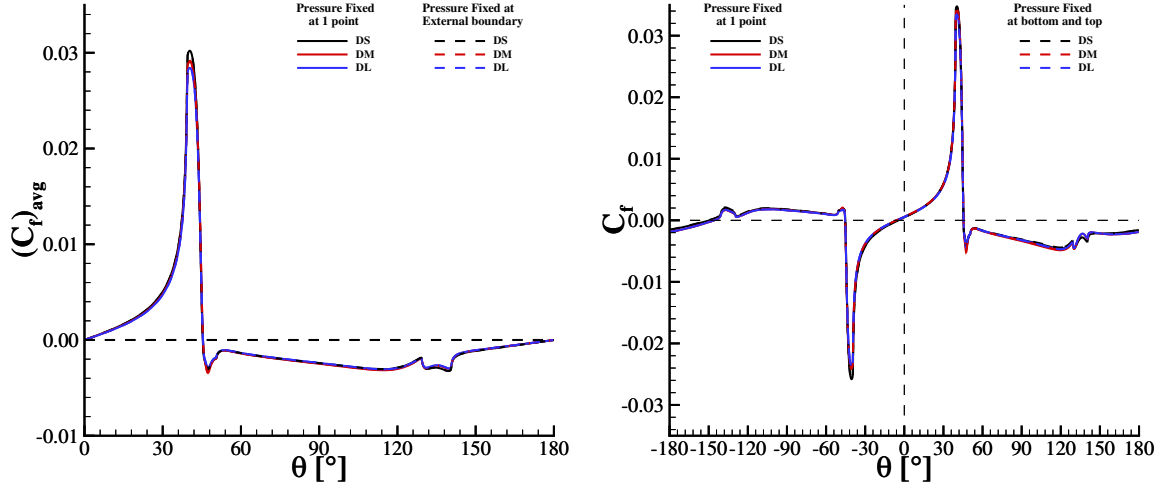


Figure 6: Skin friction coefficient  $C_f$  on the cylinder surface: average value (left); value at time corresponding to  $(C_L)_{max}$ . ( $\theta = 0$  at  $x = -0.5D, y = 0$ ,  $\theta = 180^\circ$  at  $x = 0.5D, y = 0$ ,  $\theta = -90^\circ$  at  $x = 0, y = -0.5D$  and  $C_f$  multiplied by -1 for negative  $\theta$ ). Calculation of the two-dimensional flow around a squared cylinder of rounded corners at  $Rn = 1.74 \times 10^5$  with three different sizes of the computational domain and different pressure boundary conditions. IM inlet conditions.

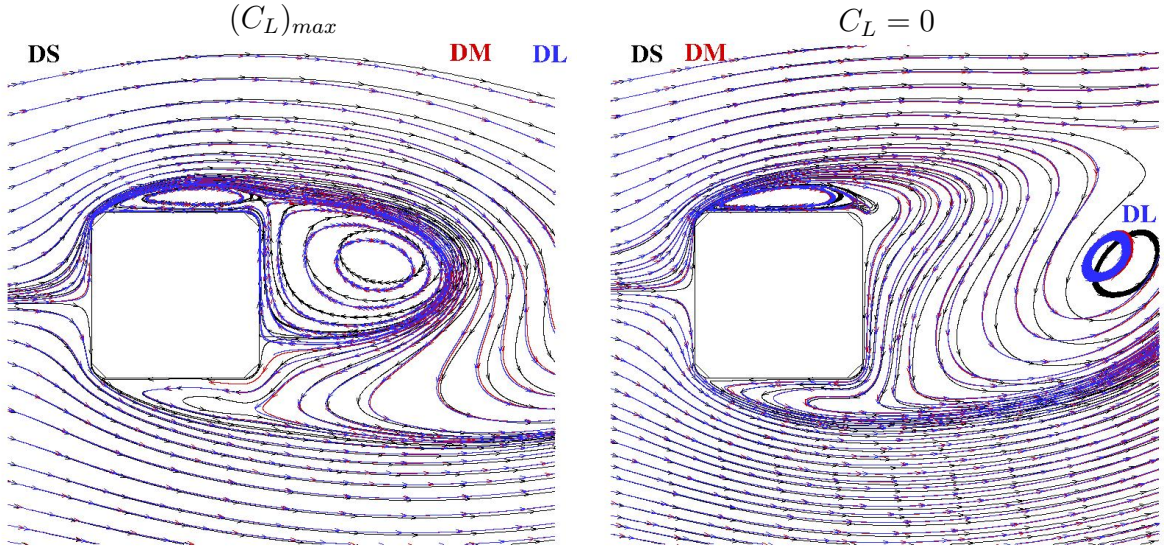


Figure 7: Streamlines at times corresponding to  $(C_L)_{max}$  (left) and  $C_L = 0$  (right). Calculation of the two-dimensional flow around a squared cylinder of rounded corners at  $Rn = 1.74 \times 10^5$  with three different sizes of the computational domain and pressure fixed at 1 point. IM inlet conditions.

on the top and bottom surfaces of the cylinder.

For the sake of completeness, figure 7 presents the streamlines at the times of maximum  $((C_L)_{max})$  and zero lift coefficient ( $C_L = 0$  and growing) for the three selected domains

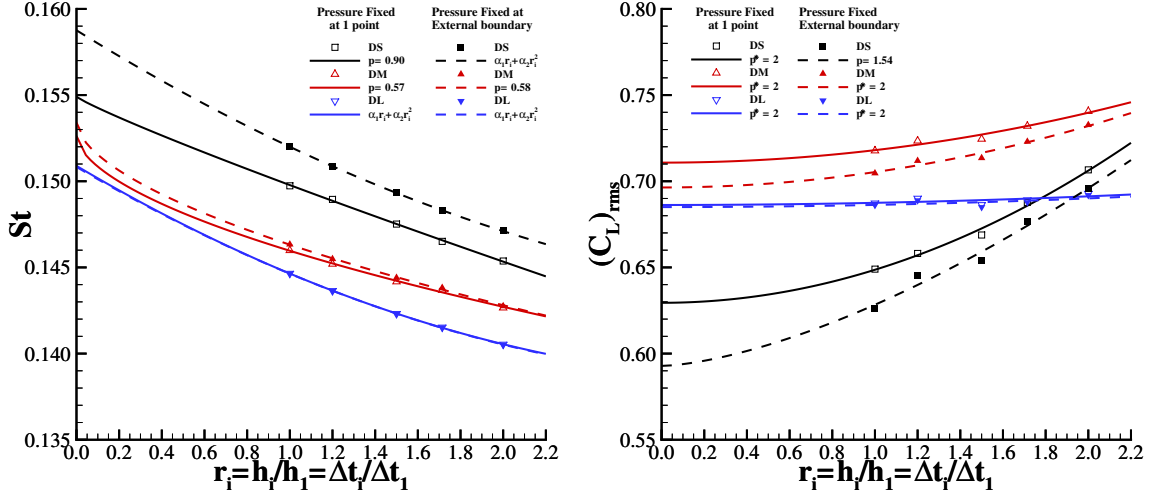


Figure 8: Strouhal number  $St$  (left) and root mean squared of the lift coefficient  $(C_L)_{rms}$  as a function of the grid/time refinement ratio (right). Calculation of the two-dimensional flow around a squared cylinder of rounded corners at  $Rn = 1.74 \times 10^5$  with three different sizes of the computational domain and different pressure boundary conditions. IM inlet conditions.

for the calculations performed with pressure fixed at the top left corner of the domain. The differences between the DS and DM domains are clearly smaller than those obtained between the DM and the DL domains. It is also clear that the near-wake of these two time instants is significantly different.

The Strouhal number  $St$  and the root mean squared of the lift coefficient  $(C_L)_{rms}$  are depicted in figure 8 as a function of the grid/time refinement ratio  $r_i$ . The change in Strouhal number with the domain size is monotonic. However, the effect of the pressure boundary conditions is mainly visible for the smallest domain DS. In fact, the change in  $St$  between domains DL and DM is smaller than the effect of the pressure boundary condition on  $St$  for the smallest domain DS. On the other hand,  $(C_L)_{rms}$  does not exhibit a monotonic change with the increase of the domain size and only the largest domain DL exhibits a negligible influence of the pressure boundary condition. Interestingly, the grid/time dependency of  $(C_L)_{rms}$  is strongly dependent on the domain size with the largest dependency obtained for the smallest values of  $(C_L)_{rms}$ .

### 4.3 Inlet turbulence quantities

The evaluation of the influence of the level of the inlet turbulence quantities (see table 2) was performed for the smallest domain DS with pressure fixed at the top left corner and for the largest domain DM with pressure fixed at the external boundary. As illustrated in the previous section, there is a negligible effect of the pressure boundary conditions in the DL domain. As discussed in section 3.2,  $\nu_t$  decays much slower than  $k$  and  $\omega$  in regions of uniform flow. Therefore, we will refer to the level of  $\nu_t$  at the inlet to identify the inlet

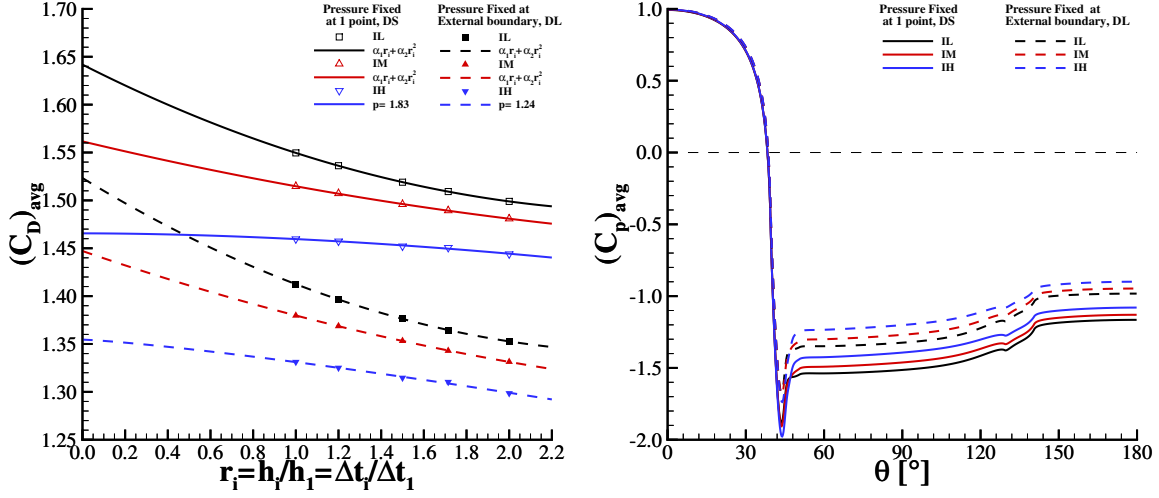


Figure 9: Average drag coefficient  $(C_D)_{avg}$  as a function of the grid/time refinement ratio (left); average surface pressure coefficient  $(C_p)_{avg}$  distribution ( $\theta = 0$  at  $x = -0.5D, y = 0$  and  $\theta = 180^\circ$  at  $x = 0.5D, y = 0$ ) for  $r_i = 1$  (right). Calculation of the two-dimensional flow around a squared cylinder of rounded corners at  $Rn = 1.74 \times 10^5$  with three different levels of the inlet turbulence quantities. Domain size and pressure boundary conditions given in the plots legend.

turbulence quantities in the discussion below.

The average drag coefficient  $(C_D)_{avg}$  as a function of the grid/time refinement ratio  $r_i$  and the average surface pressure coefficient  $(C_p)_{avg}$  distribution for  $r_i = 1$  are presented in figure 9. The influence of the inlet value of  $\nu_t$  on  $(C_D)_{avg}$  is similar in the two domains tested. There is a monotonic decrease of  $(C_D)_{avg}$  with the growth of  $\nu_t$  with largest changes between IM and IH than between IL and IM. The  $(C_p)_{avg}$  distribution shows that these differences are originated at the corner of the cylinder with very small changes in the location of the separation point producing significantly different base pressure levels.

Figure 10 presents the maximum lift coefficient  $(C_L)_{max}$  as a function of the grid/time refinement ratio  $r_i$  and the  $C_p$  surface distributions at the time corresponding to  $(C_L)_{max}$ . For both domains tested, there is a significant influence of the inlet  $\nu_t$  on the predicted  $(C_L)_{max}$ . Nevertheless, the change with the  $\nu_t$  level is monotonic. The  $C_p$  distribution at the time of maximum lift shows that the differences are again originated at the separation points of the flow with a stronger effect of the inlet  $\nu_t$  at the top corner than at the low corner.

Figure 11 presents the average skin friction coefficient  $(C_f)_{avg}$  on the cylinder surface and the  $C_f$  distribution for the time of  $(C_L)_{max}$ . Although there are some differences at the left corners of the cylinder for both distributions, the data show that the effect of the inlet  $\nu_t$  on the friction force is clearly smaller than that obtained for the pressure force.

Figure 12 presents the streamlines at the times of maximum ( $(C_L)_{max}$ ) and zero ( $C_L = 0$  and growing) lift coefficient for the three levels of inlet  $\nu_t$  obtained in the domain DS with pressure fixed at the top left corner of the domain. Although the overall pattern of the

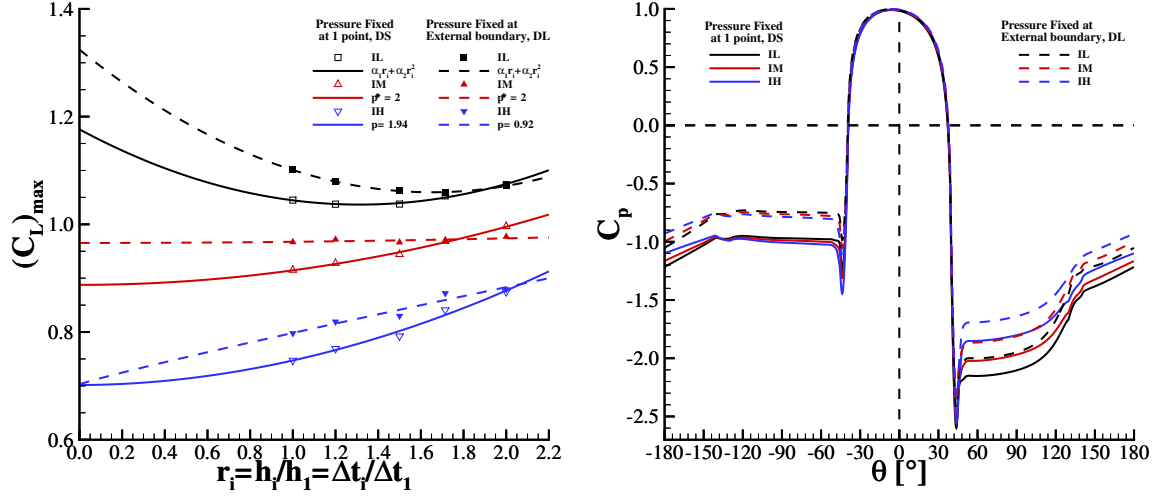


Figure 10: Maximum lift coefficient  $(C_L)_{max}$  as a function of the grid/time refinement ratio (left); surface pressure coefficient  $(C_p)_{avg}$  distribution ( $\theta = 0$  at  $x = -0.5D, y = 0$ ,  $\theta = 180^\circ$  at  $x = 0.5D, y = 0$  and  $\theta = -90^\circ$  at  $x = 0, y = -0.5D$ ) at the time corresponding to  $(C_L)_{max}$  for  $r_i = 1$  (right). Calculation of the two-dimensional flow around a squared cylinder of rounded corners at  $Rn = 1.74 \times 10^5$  with three different levels of the inlet turbulence quantities. Domain size and pressure boundary conditions given in the plots legend.

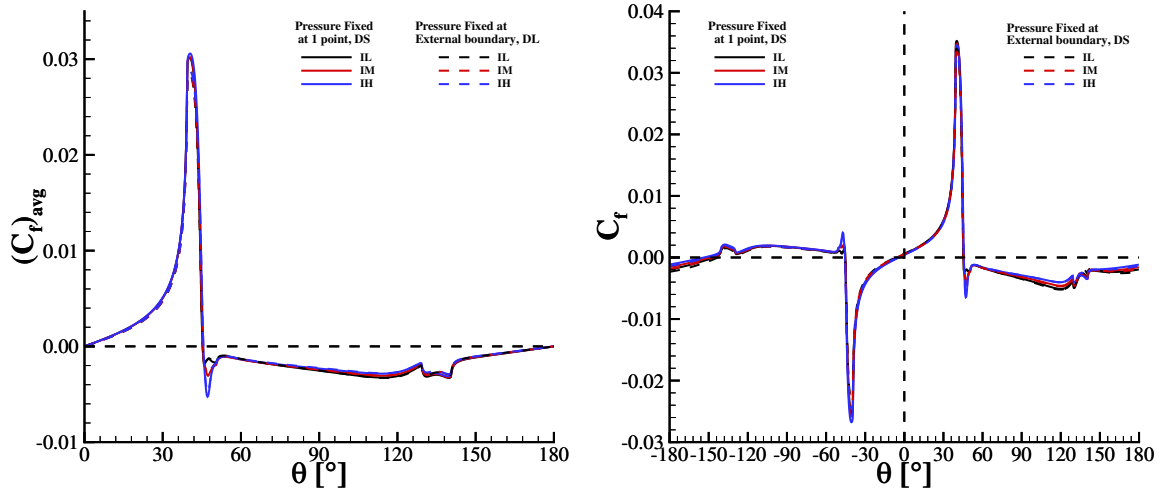


Figure 11: Skin friction coefficient  $C_f$  on the cylinder surface: average value (left); value at time corresponding to  $(C_L)_{max}$ . ( $\theta = 0$  at  $x = -0.5D, y = 0$ ,  $\theta = 180^\circ$  at  $x = 0.5D, y = 0$ ,  $\theta = -90^\circ$  at  $x = 0, y = -0.5D$  and  $C_f$  multiplied by -1 for negative  $\theta$ ). Calculation of the two-dimensional flow around a squared cylinder of rounded corners at  $Rn = 1.74 \times 10^5$  with three different levels of the inlet turbulence quantities. Domain size and pressure boundary conditions given in the plots legend.

flow is similar for the three levels of inlet  $\nu_t$  tested, there is a strong effect of the inlet turbulence quantities on the near wake for both time instants. Similar effects of the inlet



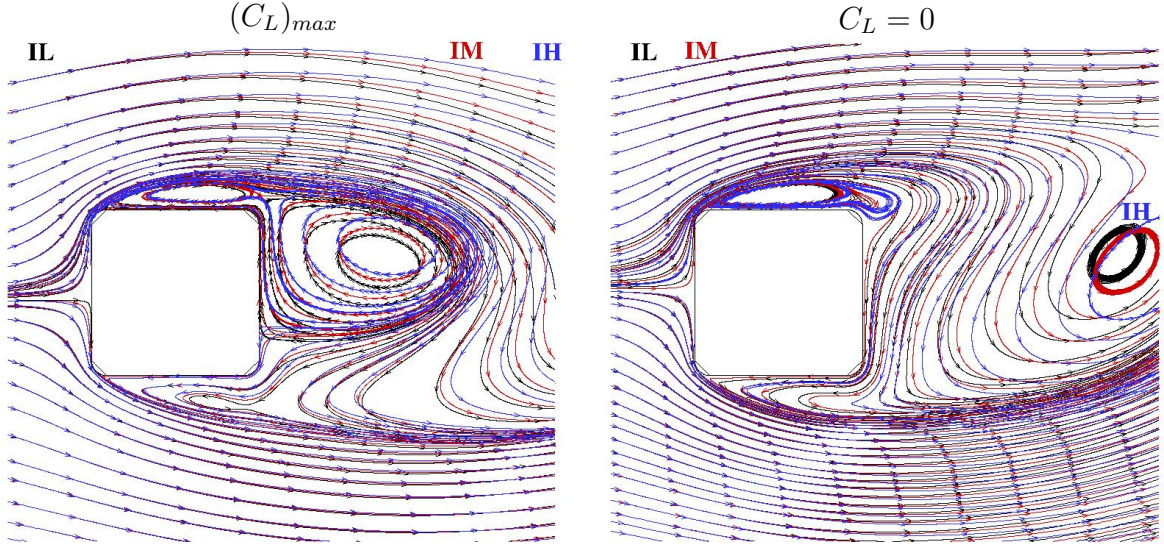


Figure 12: Streamlines at times corresponding to  $(C_L)_{max}$  (left) and  $C_L = 0$  (right). Calculation of the two-dimensional flow around a squared cylinder of rounded corners at  $Rn = 1.74 \times 10^5$  with three different levels of the inlet turbulence quantities. Smallest domain size DS with pressure fixed at 1 point.

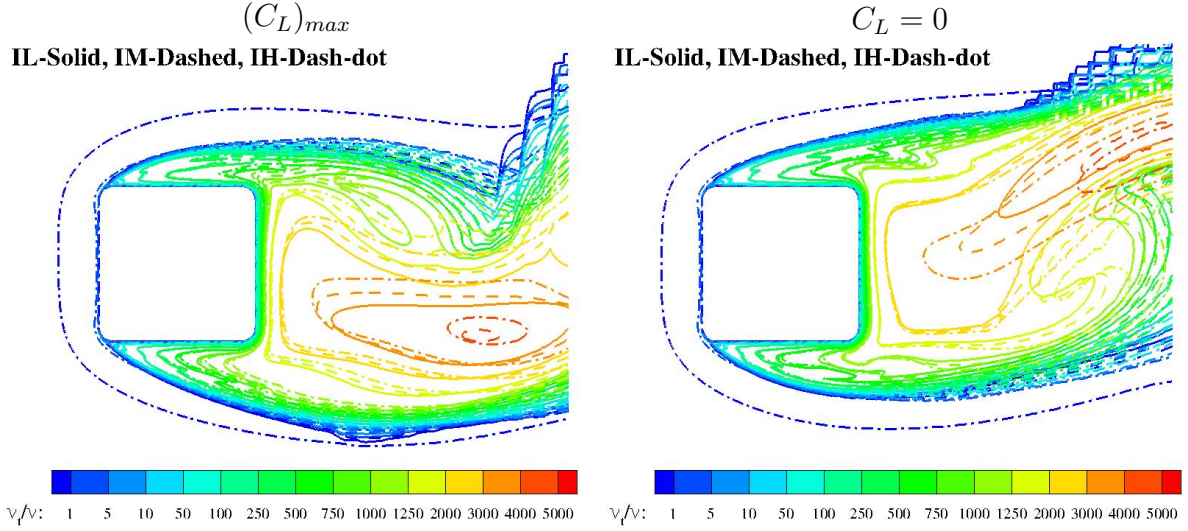


Figure 13: Eddy-viscosity ( $\nu_t$ ) isolines at times corresponding to  $(C_L)_{max}$  (left) and  $C_L = 0$  (right). Calculation of the two-dimensional flow around a squared cylinder of rounded corners at  $Rn = 1.74 \times 10^5$  with three different levels of the inlet turbulence quantities. Smallest domain size DS with pressure fixed at 1 point.

$\nu_t$  are obtained in the DL domain with pressure fixed at the external boundary.

For the sake of completeness, figure 13 present the eddy-viscosity isolines for the same time instants of figure 12 corresponding to maximum ( $(C_L)_{max}$ ) and zero ( $C_L = 0$  and

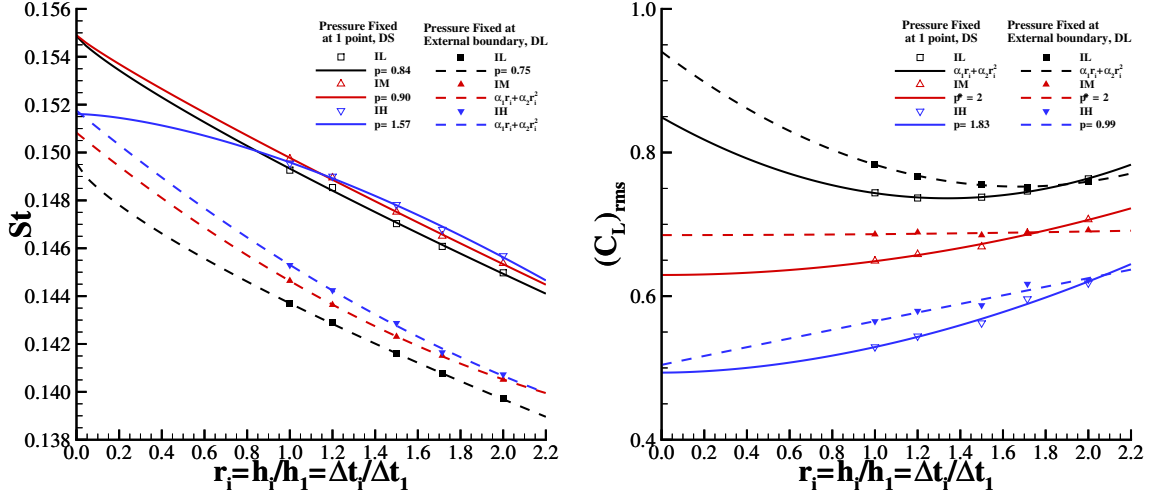


Figure 14: Strouhal number  $St$  (left) and root mean squared of the lift coefficient  $(C_L)_{rms}$  as a function of the grid/time refinement ratio (right). Calculation of the two-dimensional flow around a squared cylinder of rounded corners at  $Rn = 1.74 \times 10^5$  with three different levels of the inlet turbulence quantities. Domain size and pressure boundary conditions given in the plots legend.

growing) lift coefficient. In both time instants,  $\nu_t$  is larger than  $\nu$  upstream of the cylinder for the IH inlet boundary conditions. However, the most striking feature of the plots is the impact of the inlet turbulence quantities on the level of  $\nu_t$  in the near-wake.

Finally, figure 14 presents the Strouhal number  $St$  and  $(C_L)_{rms}$  as a function of the grid/time refinement ratio  $r_i$ . The effect of the inlet  $\nu_t$  on the Strouhal number is larger for the DL domain than for the DS domain where the differences between the three solution are clearly below the numerical uncertainty. On the other hand,  $(C_L)_{rms}$  shows a systematic decrease with the growth of the inlet  $\nu_t$  in both domains.

#### 4.4 Overall comparison

The two previous sections demonstrate that the computational domain size, pressure boundary conditions and inlet turbulence quantities may have a significant influence on the predicted flow field around a cylinder with squared corners. Table 4 presents the maximum differences obtained for the selected flow quantities in percentage of the mean value,  $\Delta\phi = 200(\phi_{max} - \phi_{min})/(\phi_{max} + \phi_{min})$ . The results are presented for changes in domain size, pressure boundary conditions and inlet turbulence quantities. The final column corresponds to the comparison of all calculations performed.

The comparison of the data included in tables 3 and 4 shows that the discrepancies between results obtained with different problem settings (table 4) are clearly larger than the data range (table 3) and most likely larger than the numerical uncertainty. It is also evident that the domain size has the strongest influence on  $(C_D)_{avg}$  and  $St$ . On the other hand, the inlet turbulence quantities lead to the largest changes on  $(C_L)_{max}$  and



$\Delta\phi(\%)$	Domain Size	Pressure Boundary Condition	Inlet Turbulence Quantities	Global
$(C_D)_{avg}$	9.33	0.1	5.98	15.2
$(C_L)_{max}$	11.6	3.47	31.9	38.3
$(C_L)_{rms}$	11.8	3.61	32.4	38.7
$St$	4.96	1.50	1.11	5.63

Table 4: Largest differences of average drag coefficient  $(C_D)_{avg}$ , maximum  $(C_L)_{max}$  and root mean squared  $(C_L)_{rms}$  lift coefficient and Strouhal number  $St$ . Calculation of the two-dimensional flow around a squared cylinder with rounded corners at  $Re = 1.74 \times 10^5$  with different domain sizes, pressure boundary conditions and inlet turbulence quantities.

$(C_L)_{rms}$ . The pressure boundary conditions have the smallest influence on the selected flow quantities.

## 5 CONCLUSIONS

This paper addresses the effect of the problem settings, i.e. the domain size, pressure and inlet turbulence quantities boundary conditions, on the calculation of the flow around a squared cylinder with rounded corners. The flow is predicted with one of the simplest mathematical models available: two-dimensional, incompressible, Reynolds-averaged Navier-Stokes equations supplemented with the SST  $k - \omega$  eddy-viscosity model. Naturally, ensemble average has been applied due to the periodic nature of the flow.

The selected flow quantities are the average drag coefficient, the maximum and root mean squared lift coefficient and the Strouhal number. Besides these functional quantities, the surface distributions of the pressure and skin friction coefficients are also analyzed to understand the origin of the discrepancies obtained in the force coefficients.

Grid/time refinement studies are performed for all choices of the problem settings to enable the estimation of the numerical uncertainty. Unfortunately, the level of grid/time refinement of the coarsest grids (840 or less cells on the surface of the cylinder) is too coarse to obtain reliable estimates of the numerical uncertainty based on power series expansions. Nonetheless, the data suggest that the sharp gradients of the pressure and skin friction coefficients at the flow separation points (left corners of the cylinder) require extremely dense grids to obtain negligible numerical uncertainties.

From the three problem settings tested, the pressure boundary conditions exhibit the smallest influence on the selected flow quantities. Nonetheless, it is clear that the choice of pressure boundary conditions becomes more important with the reduction of the domain size. On the other hand, the domain size and the inlet turbulence quantities have a significant influence on the simulation results. Furthermore, the effect of these choices is not identical for all the selected flow quantities. Domain size leads to the strongest influence on the average drag coefficient and Strouhal number, whereas the inlet turbulence quantities show the largest effect on the maximum and root mean squared lift coefficient.

It may be argued that the effect of the domain size in two-dimensional simulations is stronger than in three-dimensional flows. However, most likely, the width of the domain will also affect the flow simulations. Additionally, there is no reason to expect that the influence of the inlet turbulence quantities for three-dimensional and/or more sophisticated mathematical models is smaller than that obtained in this study. Therefore, reliable comparisons of simulations with experiments, i.e. serious validation exercises, are troublesome to perform without correct domain sizes and/or boundary conditions. Unfortunately, many experiments available in the open literature do not provide all the required information, especially the turbulence quantities boundary conditions.

## REFERENCES

- [1] Zdravkovich M.M. - *Flow Around Circular Cylinders: Volume I: Fundamentals* - OUP Oxford, April 1997.
- [2] Carassale, L., Freda, A., Marr-Brunenghi, M., Piccardo, G., Solari, G. - *Experimental investigation on the aerodynamic behavior of square cylinders with rounded corners* - The Seventh International Colloquium on Bluff Body Aerodynamics and Applications (BBAA7), 2-6 September 2012, Shanghai, China.
- [3] Carassale, L., Freda, A., Marr-Brunenghi, M., - *Experimental investigation on the aerodynamic behavior of square cylinders with rounded corners* - Journal of Fluids and Structures, Journal of Fluids and Structures Vol. 44, 2014, pp. 195-204.
- [4] Carassale, L., Freda, A., Marr-Brunenghi, M. - *Effects of free-stream turbulence and corner shape on the galloping instability of square cylinders shapes*. Journal of Wind Engineering and Industrial Aerodynamics Vol. 123, 2013, pp.274-280.
- [5] Delany, N.K., Sorensen, N.E. - *Low-Speed Drag of Cylinders of Various Shapes*. Technical note 3038. National Advisory Committee for Aeronautics. 1953.
- [6] Tamura, T., Miyagi, T., Kitagishi, T., - *Numerical prediction of unsteady pressures on a square cylinder with various corner shapes* - Journal of Wind Engineering and Industrial Aerodynamics 74-76, 1998, pp. 531-542.
- [7] Tamura, T., Miyagi, T. - *The effect of turbulence on aerodynamic forces on a square cylinder with various corner shapes* - Journal of Wind Engineering and Industrial Aerodynamics Vol. 83, 1999, pp. 135-145.
- [8] Letchford, C., Mason, M. - *Drag of square section tubes*. In 13th International Conference on Wind Engineering, 10-15 July 2011, Amsterdam, Netherlands.
- [9] Helder J. H., Tap F. - *ARD Square Cylinder Forced Oscillation tests 2011* - MARIN Report 70023.153-1-HT, July 2011.

- [10] Menter F.R. - *Two-Equation Eddy-Viscosity Turbulence Models for Engineering Applications* - AIAA Journal, Vol.32, August 1994, pp. 1598-1605.
- [11] Eça L., Hoekstra M., *A procedure for the estimation of the numerical uncertainty of CFD calculations based on grid refinement studies*, Journal of Computational Physics, Vol. 261 April 2014, pp-104-130.
- [12] ReFRESHCO, <http://www.refresco.org>, 2015.
- [13] Eça L, Hoekstra M. - *On the Grid Sensitivity of the Wall Boundary Condition of the  $k - \omega$  model* - Journal of Fluids Engineering, Vol. 126,Nº 6, November 2004, pp. 900-910.